Article

A Molecular Modeling Study into Brønsted and Lewis Acid Catalyzed Conversion of CBD into Other Cannabinoids

Wim Buijs 🆔

Process & Energy Department, Faculty of Mechanical, Maritime and Materials Engineering, Delft University of Technology, 2628 CB Delft, The Netherlands; wbuijsm@gmail.com; Tel.: +31-630657250

Abstract: There is a continuous interest in cannabinoids like Δ^9-tetrahydrocannabinol (Δ^9-THC) and cannabidiol (CBD). Previous experimental research has described the conversion of CBD to either Δ^8-THC or Δ^9-THC, depending on the acid catalyst applied. The use of para-toluene sulfonic acid (pTSA) has led to the formation of Δ^8-THC, while boron trifluoride etherate (BF$_3$·Et$_2$O) has mainly yielded Δ^9-THC. The enormous difference in product selectivity between these two catalysts was investigated with Molecular Modeling, applying quantum chemical density functional theory. It was found that pTSA leads to fast isomerization of Δ^9-CBD to Δ^8-CBD and subsequent ring closure to Δ^8-THC. BF$_3$·Et$_2$O catalysis leads to the formation of tertiary carbenium ions in the transition states, which yield Δ^9-THC and some iso THC. Under dry conditions in refluxing toluene, it was found that pTSA is predominantly present as a dimer, and only a small fraction is available as monomeric catalyst. Applying the computationally derived activation barriers in transition state theory yielded reaction rates that predicted the amounts of cannabinoids that are in close agreement with the experimental findings from the previous literature.

Keywords: cannabinoids; density functional theory; transition state theory

1. Introduction

There is continuous interest in cannabinoids like Δ^9-tetrahydro cannabinol (Δ^9-THC) and cannabidiol (CBD), which are the two most important cannabinoids [1,2]. CBD has a different medical and pharmacological profile than Δ^9-THC. CBD is a promising candidate drug that shows analgesic, anticonvulsant, muscle relaxant, anxiolytic, antipsychotic, neuroprotective, anti-inflammatory, and antioxidant activity [3–5]. At the same time, it does not show psychotropic effects like Δ^9-THC.

However, the interest in CBD is not only explained by its favorable medical and pharmacological profile but also by its potential to be converted to Δ9-THC [2,6], which has caused controversy in the scientific literature. The latter can be easily understood, as CBD accounts for 40% of the cannabis plant extract [3].

Finally, in 2020, the UN, recognizing their medical applications, has reclassified cannabinoids and removed them from a list of potential very harmful products like various opioids [2,7]. This has undeniably led to renewed interest from the pharmaceutical industry in lesser-known cannabinoids because of possible new pharmacological profiles and the associated patentability, either of the substances or good synthetic routes. Still, it is strongly advised to use any cannabinoid on explicit medical prescription only.

In 2004, a patent application by Webster et al. was published, and in 2008, it was followed by the granted patent describing the catalytic conversion of CBD to either Δ8-THC or Δ9-THC, depending on the acid catalyst applied [8,9]. The use of Brønsted acid para-toluene sulfonic acid (pTSA) led to the formation of Δ^8-THC, while the use of Lewis acid boron trifluoride etherate (BF$_3$·Et$_2$O) yielded mainly Δ^9-THC and some iso THC. These patents are important as Δ^8-THC, showing a similar pharmacological profile as Δ^9-THC, might exhibit a lower psychotropic effect, while the effects of iso THC are largely

unknown [10]. Furthermore, the enormous difference in product selectivity between these two catalysts is intriguing and worth investigating. In this molecular modeling study, the mechanisms of the Brønsted and Lewis acid catalyzed conversion of CBD into other cannabinoids are investigated, and the computational results are compared with the experimental data of Webster et al.

2. Materials and Methods

All molecular modeling work was performed with Spartan'20 [11]. Spartan'20 includes most, but not all academic quantum mechanical and molecular mechanics codes. Merck forcefield (MMFF) is one of the most widely used molecular mechanics methods. MMFF is extensively described by Halgren et al. [12–16]. The general computational approach can be described in three steps:

1. Finding suitable geometries;
2. Full geometry optimization;
3. Determination of properties.

1. Finding suitable geometries.

MMFF was used to explore the conformational flexibility of the various cannabinoids by performing conformer distribution (CD) calculations, a defined computational task in Spartan'20, which also includes their Boltzmann weights. Until now, molecular mechanics MMFF usually does a better job with respect to the relative energies of possible conformers and computational time than QM methods.

2. Full geometry optimization.

The outcomes of molecular mechanics were used to perform quantum chemical calculations at the density function level. All structures underwent full geometry optimization, applying B3LYP/6-31G*. This DFT functional is one of the most validated methods. Other DFT functionals like the popular ωB97X-D or MO6-2X lead to similar results.

3. Determination of properties.

B3LYP/6-31G* derived the total energies from geometry optimizations, and enthalpy corrections were used to calculate approximate reaction energies and activation barriers. This requires a frequency calculation for each structure. Furthermore, it was assumed that the calculated reaction and activation enthalpies are a reasonable approach for reactions and activation energies. Entropy corrections were not made due to the huge simplifications made in the systems already. One of the results of the transition state calculation is a unique imaginary vibrational frequency. The animation of this unique imaginary vibrational frequency should show the desired movement of the atoms during the reaction. Isodesmic reactions [17] were used whenever possible. The resulting cancelation of methodological or code errors minimizes the error to a value lower than ±5 kJ/mol. Rate constants were calculated, using transition state theory [18] by applying the simplified expression:

$$k = k_B \cdot T/h \cdot e^{-\Delta Ha/RT} \text{ originating from } k = \kappa \cdot k_B \cdot T/h \cdot e^{-\Delta Ga/RT}$$

To arrive at the simplified expression, additional approximations are that the transmission coefficient k = 1 and $\Delta G_a \sim \Delta H_a$, the latter of which is in line with the fact that only enthalpy corrections were made.

In the case of catalysis with the Lewis acid $BF_3 \cdot Et_2O$, the pK_a value of $ArOH-BF_3$ was calculated, applying an earlier reported relation between the maximum electrostatic potential (MEP) at the isodensity surface: 0.002 e/au^3 and pK_a [19]. By taking structurally similar sulfonic acids with experimentally known pK_as, its accuracy was further increased.

3. Results

3.1. Experimental Results

Webster et al. describe in their patents [8,9] only two examples, both of which are of crucial interest for this study.

Example 1 describes the conversion of Δ^9-CBD to Δ^8-THC using dry pTSA as a catalyst in refluxing toluene (110.6 °C). The progress of the reaction was monitored with HPLC. After 15 min, 79.3% of Δ^8-THC was formed, after 30 min, 81.7% was formed, after 60 min, 86.0% was formed, and finally, after 120 min, 84.6% was formed. No other products are mentioned explicitly, but column chromatography yielded 81% Δ^8-THC with a purity of 98.6%. Therefore, the byproduct most likely is Δ^9-THC because it is known that Δ^8-THC and Δ^9-THC are very difficult to separate completely [2]. It is mentioned that toluene is the best solvent and that dry pTSA was used. It seems that conversion is essentially almost complete after 60 min.

Example 2 describes the conversion of CBD to Δ^9-THC using $BF_3.Et_2O$ as a catalyst in dichloromethane at 0 °C. According to HPLC, 27.0% of iso THC and 66.7% of Δ^9-THC was formed after 60 min. In contrast to example 1, the progress of the reaction was not specified further. However, as the sum of the products accounts for almost 94%, conversion must be almost complete.

3.2. Computational Results

3.2.1. Cannabinoid Structures

To avoid confusion, the structures of all relevant cannabinoids are shown in Figure 1 and shortly discussed below.
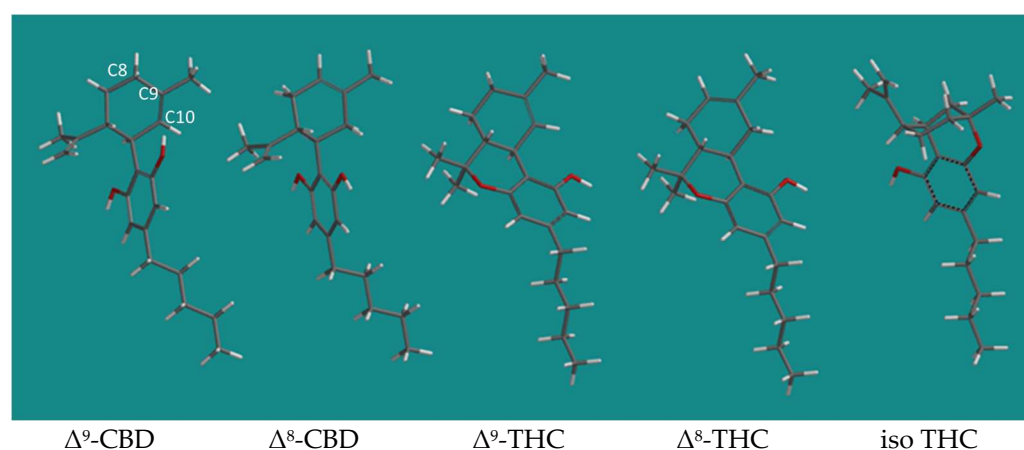

Figure 1. The structure of Δ^9-CBD, Δ^8-CBD, Δ^9-THC, Δ^8-THC, and iso THC. Display: tube; C: black, H: white, O: red. The positions of atoms C8, C9, and C10 are indicated in white at the structure of Δ^9-CBD.

The structures of Δ^9-CBD, Δ^8-CBD, Δ^9-THC, and Δ^8-THC have been extensively discussed before [6] and originate from CD calculations, as described in the Materials and Methods section. To clarify the discussion, the positions of the carbon atoms C8, C9, and C10 are indicated in Δ^9-CBD. For readers who appreciate the more classical representation of the structures in 2D, Golombek et al., [2] provide a good overview of all structures in their Figure 4 and a complete numbering of all C-atoms in their Figure 1. Because the C_5 alkyl side chain is not directly important for the ring closure and isomerization reactions of the cannabinoids, a smaller cannabinoid model with a methyl group as the side chain was chosen to reduce the very high number of possible conformers. The same approach was adopted for iso THC, using a model in which the C_5 chain was reduced to a methyl group too. Like Δ^9-THC and Δ^8-THC, the conformational freedom of iso THC is restricted by the ring closure of the phenolic group to the C9 of the (former) cyclohexenyl substituent and shows only 13 conformers, all of them with the newly formed cyclohexane ring in a chair position with three axial substituents: the C-C(Ar)-, the C-O(Ar)-, and the isopropenyl substituent. Only the $C-CH_3$ at the C9 position is in an equatorial position. The main differences between the conformers are in the position of the remaining phenolic group and the orientation of the isopropenyl substituent. The best conformer, which is

in this case the most abundant and lowest energy conformer, accounts for 84.6% of the Boltzmann weights, and the second-best conformer, showing a phenol group pointing to the isopropenyl cyclohexane substituent, accounts for 6.6% of the Boltzmann weights.

3.2.2. The Conversion of Δ^9-CBD to Δ^8-THC, with pTSA as Brønsted Acid Catalyst

The conversion of Δ9-CBD to Δ8-THC, with pTSA as Brønsted acid catalyst, requires two steps: ring closure and isomerization of the double bond from the Δ9 to the Δ8-position. The order of the two reactions is not clear in advance, so both options will be investigated. For both cases firstly the ring closure reactions will be discussed and next the isomerization reactions. A choice between the options will be made in Section 3.2.4. Kinetic models: comparison of computational and experimental results.

Ring Closure of Δ^9-CBD to Δ^9-THC and Δ^8-CBD to Δ^8-THC Catalyzed by pTSA

Ring closure reactions catalyzed by pTSA are quite rare. A recent example can be found in the pTSA condensation polymerization of dicarboxylic acids and polyols like sorbitol, where it appears as a side reaction on a secondary carbon atom [20]. Ring closure by a phenol on a tertiary carbon seems possible only because of the intramolecular presence of the phenolic group, the absence of more suitable nucleophiles, and activation of the alkene by pTSA. These conditions are fulfilled by the reaction conditions described above; dry pTSA is used as a catalyst in refluxing toluene. Figure 2 shows details of the transition states of the ring closure of Δ^9-CBD to Δ^9-THC and Δ^8-CBD to Δ^8-THC catalyzed by pTSA. The corresponding starting complexes are not shown but can be easily imagined from the transition states. The main difference is in the position of the proton on pTSA. In the starting complexes, the H-OSO$_2$Ar-pCH$_3$ distance is ~0.990 Å and the H$_2$C-HOSO$_2$Ar-pCH$_3$ distance is ~2.25 Å.
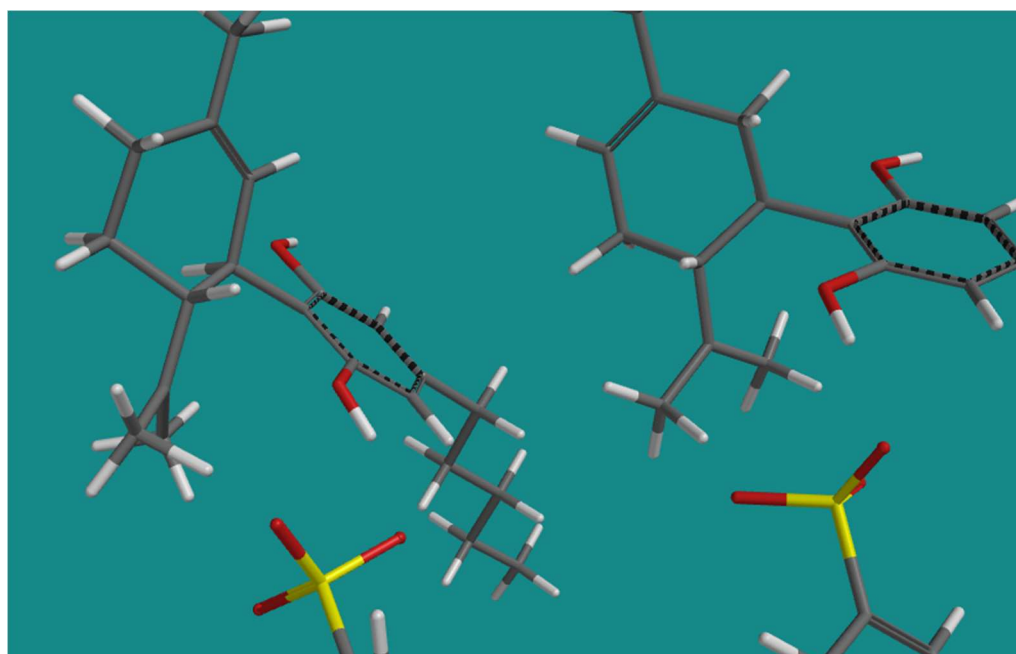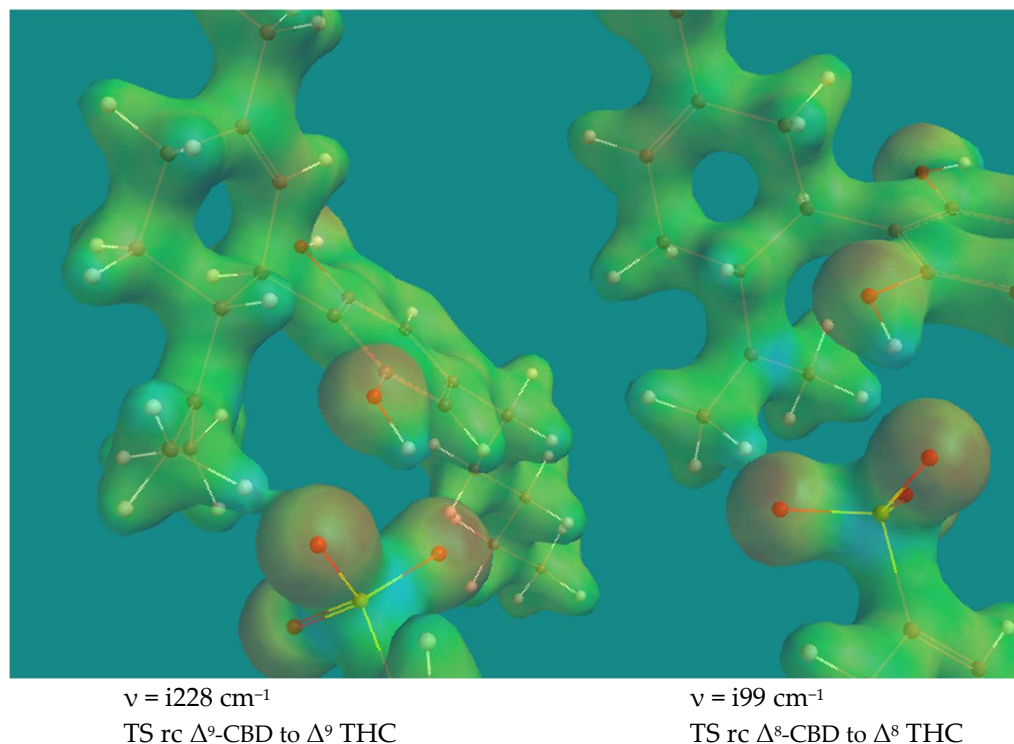

Figure 2. *Cont*.

$\nu = i228\ cm^{-1}$ $\nu = i99\ cm^{-1}$

TS rc Δ^9-CBD to Δ^9 THC   TS rc Δ^8-CBD to Δ^8 THC

Figure 2. Details of the transition states ring closure of Δ^9-CBD to Δ^9-THC and Δ^8-CBD to Δ^8-THC catalyzed by pTSA. B3LYP/6-31G* Display: tubes, ball and wire with transparent surfaces; reduced electron density = 0.08 e/au^3, projected property on electron density: electrostatic potential, range: -200 (red)–+2000 (blue) kJ/mol.

The two transition states look very similar. There is almost complete proton transfer from pTSA to the CH$_2$ of the isopropenyl group; the CH$_2$–HOSO$_2$Ar–pCH$_3$ distance is 1.237 Å and 1.212 Å. This is also visible from the reduced electron density plot (electron density = 0.08 e/au^3). Such a plot provides a good indication of the character of the chemical bond. The more visible the electron density, the more covalent the character of the chemical bond, while the absence of electron density indicates a more ionic character. The blue color (positive electrostatic potential) indicates that the transferred particle is a proton. The phenolic O-atom is poised to form a C–O bond with the tertiary C of the isopropenyl group despite the relative long distance between them, which is 2.758 Å and 3.204 Å. The electrostatic potentials on the reduced electron density surface of the tertiary Cs are +1594 and +1544 kJ/mol, which is a clear indication of their carbocation character. Animation of both imaginary frequencies show the right movement of all atoms involved. The H-atom of the phenol group is H-bridged to an O-atom of pTSA with distances of 1.723 Å and 1.746 Å. The activation barriers are 70.5 and 57.5 kJ/mol, the latter of which is a reflection of the relative stability of Δ^9-CBD compared to Δ^8-CBD, which is 11.8 kJ/mol in favor of Δ^9-CBD.

Isomerization of Δ^9-CBD to Δ^8-CBD and Δ^9-THC to Δ^8-THC by pTSA

For the isomerization reaction, two mechanisms were considered:

(a)   a concerted process with simultaneous proton transfers from pTSA to C10 and C8 to pTSA; and

(b)   a two-step process, starting with proton transfer from pTSA to C10, followed by proton transfer from C8 to pTSA.

These mechanistic proposals for acid-catalyzed isomerization are not new but go back to 1932 [21,22], and evidence has been obtained for both cases, depending on specific reaction conditions and catalysts. Figure 3 shows the details of the transition states of the concerted and two-step processes of the isomerization of Δ^9-CBD to Δ^8-CBD with pTSA.
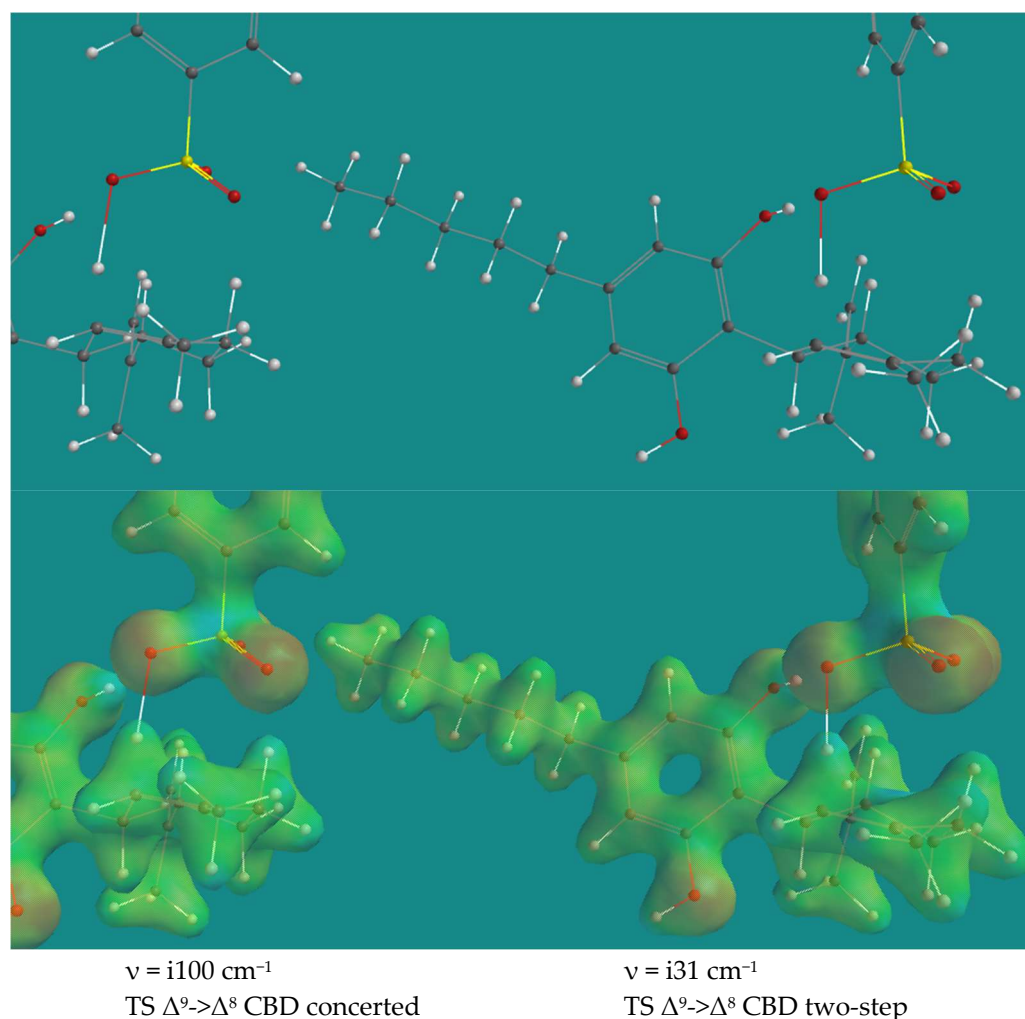
ν = i100 cm^{-1}
TS Δ^9->Δ^8 CBD concerted

ν = i31 cm^{-1}
TS Δ^9->Δ^8 CBD two-step

Figure 3. Details of the transition states isomerization of Δ^9-CBD to Δ^8-CBD with pTSA via a concerted and a two-step mechanism. B3LYP/6-31G* Display: tubes, ball and wire with transparent surfaces; reduced electron density = 0.08 e/au^3, projected property on electron density: electrostatic potential, range: −200 (red)–+2000 (blue) kJ/mol.

On first sight, the two transition states look very similar; however, their appearances are deceptive. In the concerted process, proton transfer from pCH$_3$ArSO$_3$H to C10 is almost complete with an SO–H distance of 1.911 Å and a C10–H distance of 1.126 Å, while the SO–HC8 distance is 1.720 Å and the C8–H distance is 1.169 Å. In the two-step process, proton transfer from pCH$_3$ArSO$_3$H to C10 is less complete with an SO–H distance of 1.621 Å and a C10–H distance of 1.199 Å. Note that in this case, the SO–H C8 distance is 2.175 Å and the C8–H distance is 1.112 Å, also quite different from the concerted case. Once again, the imaginary frequencies are low, and the one for the two-step process is even very low, but it shows the correct movement in both cases. The activation barriers are 75.3 and 67.2 kJ/mol. The two-step process is clearly favored over the concerted process. The starting complex for both processes is the same. The activation barriers for the reverse process, the isomerization of Δ^8->Δ^9 CBD, show significantly higher activation barriers of 93.4 and 81.8 kJ/mol. The reason for that is the higher stabilization enthalpy of the starting complex caused by the H-bridge of the phenol group of Δ^8 CBD to an O=S of pTSA, compared to the H-bridge of that phenol group of Δ^9 CBD to an HO–S of pTSA.

For the isomerization of Δ^9 THC and Δ^8 THC again the two previous mentioned options were considered. However, it turned out that for the concerted option, only a true transition state could be established, despite many attempts to locate a transition state for the two-step process. These attempts either led to the transition state of the concerted

process or to non-converged structures, which can be described best as intimate ion pairs consisting of the THC C9 cation and the pTSA anion with no imaginary frequency left and a total energy of 1–3 kJ/mol higher than the energy of the transition state of the concerted process. In the concerted process, proton transfer from pCH_3ArSO_3H to C10 is almost complete with an SO–H distance of 1.836 Å and a C10–H distance of 1.146 Å, while the SO–H C8 distance is 1.755 Å and the C8–H distance is 1.162 Å. The imaginary frequency is i152 cm^{-1} and its animation shows the correct movement of the proton transfers and the corresponding skeletal adaptation. The activation barriers for the TS Δ^9->Δ^8 THC and Δ^8->Δ^9 THC are 95.7 and 103.9 kJ/mol, reflecting the relative stabilities of Δ^9 and Δ^8 THC.

3.2.3. The Conversion of Δ^9-CBD to Δ^8-THC, with $BF_3 \cdot Et_2O$ as Lewis Acid Catalyst

Although $BF_3 \cdot Et_2O$ is a well-known catalyst, it is difficult to find examples in which either the ring closure of an O-nucleophile or alkene isomerization is described. Closest to the actual $BF_3 \cdot Et_2O$-catalyzed ring closure reactions are the inverse reactions, the $B(C_6F_5)_3$-catalyzed ring opening of a 2,2-disubstituted oxetane to a homoallylic alcohol and the $BF_3 \cdot Et_2O$ catalyzed decomposition of a t-butyldimethylsilyl ether originating from a tertiary alcohol [23,24]. The latter is close to Example 2 from Webster et al. [8,9], as described in 3.1 Experimental Results. In 2022, an example of alkene isomerization with $B(C_6F_5)_3$ was published, including a mechanistic description [25]. They found experimental and computational evidence that the isomerization of 2-propenyl benzene occurs via direct hydride abstraction by $B(C_6F_5)_3$ leading to a mixed allylic-benzylic carbenium ion and a 1,2-hydride shift to the terminal alkene-$B(C_6F_5)_3$ complex. They used the M06-2X DFT functional with an extended basis set and a solvation model. Unfortunately, the computational data are not available in their Supplementary Materials. Attempts to locate similar transition states with BF_3 using either the M06-2X or the B3LYP functional were not successful.

Because electron-deficient BF_3 wants to interact with electron rich systems, the complexation of BF_3 with the alkene and phenol groups of Δ^9 CBD was investigated to obtain an impression of the complexation energy. Results are listed in Table 1. As a reference, $BF_3 \cdot Et_2O$ is listed too.

Table 1. Overview interaction enthalpy (B3LYP/6-31G*; kJ/mol) of various BF_3 complexes.

Complex	Interaction Enthalpy (kJ/mol)
$BF_3 \cdot O\text{-}Et_2O$	−23.1
$BF_3 \cdot 2\text{-propenyl } \Delta^9$ CBD	−18.8
$BF_3 \cdot$ cyclohexenyl Δ^9 CBD	+1.4
$BF_3 \cdot O\text{-phenol } \Delta^9$ CBD (Δ9-THC)	−39.1
$BF_3 \cdot O\text{-phenol } \Delta^9$ CBD (iso THC)	−26.9
$BF_3 \cdot O\text{-pyran } \Delta^9$ THC	−24.3
$BF_3 \cdot O\text{-pyran iso THC}$	−26.6

From Table 1, it is clear that complexation of BF_3 with a phenol group is favored over complexation with alkenes like the 2-propenyl substituent on the cyclohexene ring, the cyclohexenyl double bond or ethers like in $BF_3 \cdot Et_2O$, $BF_3 \cdot \Delta^9$ THC, and $BF_3 \cdot$iso THC. It was observed that complexation of BF_3 with the cyclohexenyl double bond is particularly unfavorable due to steric hindrance of the methyl and 2-propenyl groups on the cyclohexenyl ring. Furthermore, complexation of BF3 with diethyl ether or pyran ethers in the products leads to similar interaction energies. Finally, it was realized that complexation of the Lewis acid BF_3 with a phenol transforms the weakly acidic phenol into a strong Brønsted acid. Figure 4 shows the simple $BF_3 \cdot$phenol complex with an electron density plot (electron density = 0.002 e/au^3). The latter coincides with the classical vanderWaals size of molecules. On the surface, the electrostatic potential is plotted. There is a clear blue spot on the surface of the phenolic group, which is indicative of a positive electrostatic

potential and related Brønsted acidity. The maximum electrostatic potential (MEP) shows a value of +314.7 kJ/mol. Using an earlier derived linear relation [26] between MEP and pK_a yielded -2.17 as an estimate for the pK_a of the $BF_3\cdot$phenol complex, which is more acidic than pTSA (MEP = +261.6 kJ/mol; $pK_a = -1.34$) and slightly less acidic than H_2SO_4 (MEP = +327.0 kJ/mol; $pK_a = -2.49$).
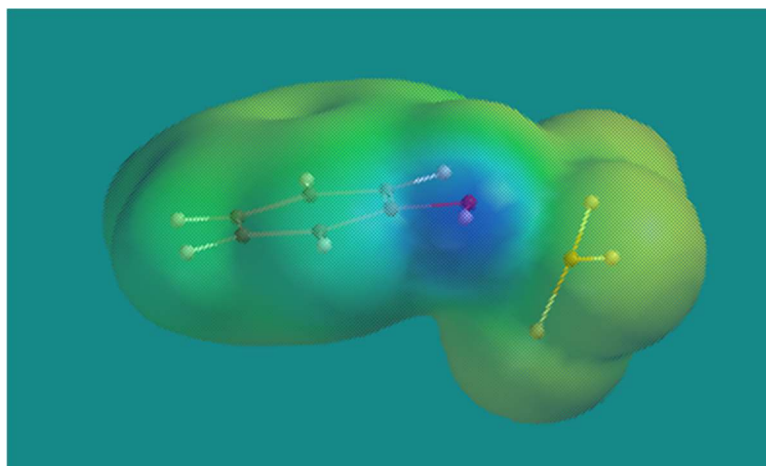

Figure 4. $BF_3\cdot$phenol complex. B3LYP/6-31G* Display: ball and wire with transparent surface; electron density = 0.002 e/au^3, projected property on electron density: electrostatic potential, range: -200 (red)–+300 (blue) kJ/mol.

Thus, reactions starting from a BF_3-phenolic cannabinoid complex were investigated. Figure 5 shows the details of the transition states of the ring closure to Δ^9-THC and iso THC.

Both transition states show nearly complete proton transfer from the phenol to the CH_2 of the 2-propenyl substituent and C8 of the cyclohexenyl substituent. Their O–H, H_2–H and O–H, OH–C8 distances are 1.850 Å, 1.142 Å and 1.743 Å, 1.157 Å, and their activation barriers are 80.9 and 82.1 kJ/mol, respectively. The animation of their imaginary frequencies clearly shows the proton transfer process and some skeletal adaptation to the formation of the tertiary carbenium ion, centered on C9. Neither a movement of the phenolic O to the tertiary C9 nor a sign of double bond isomerization are visible. Therefore, so-called energy profiles (EPs) were constructed, starting from the geometry of the transition states and leading to either the geometry of the starting $BF_3\cdot\Delta^9$-CBD complex, the $BF_3\cdot\Delta^9$-THC complex, the $BF_3\cdot$iso THC complex, or the double bond isomerized product complexes.

Figure 5. *Cont.*

$\nu = \text{i}125 \text{ cm}^{-1}$ $\nu = \text{i}315 \text{ cm}^{-1}$

TS rc Δ^9-THC   TS rc iso THC.

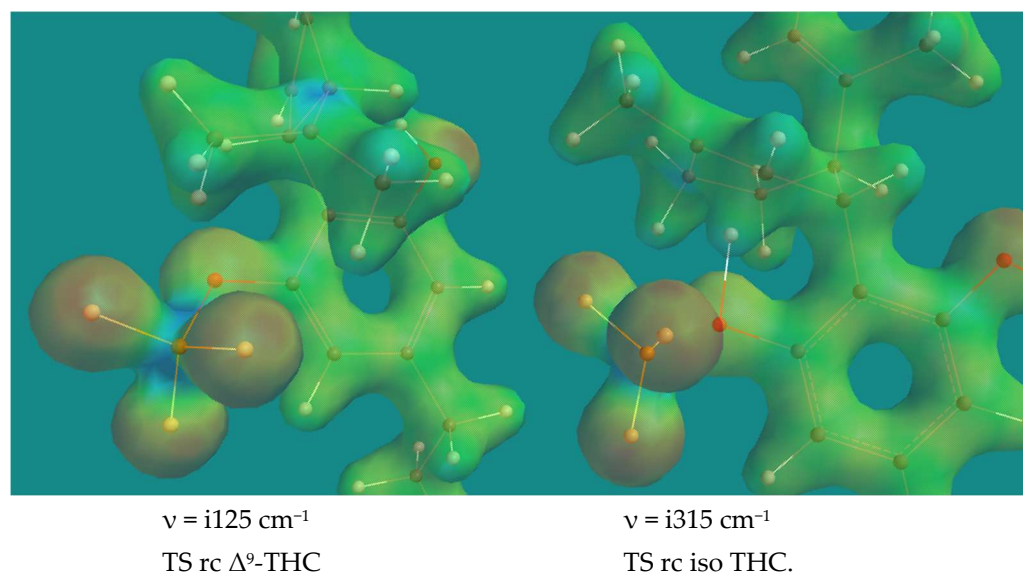**Figure 5.** Details of the transition state ring closure of $BF_3 \cdot \Delta^9$-CBD to Δ^9-THC and $BF_3 \cdot \Delta^9$-CBD to iso THC. B3LYP/6-31G* Display: tubes, ball and wire with transparent surfaces; reduced electron density = 0.08 e/au^3, projected property on electron density: electrostatic potential, range: -200 (red)–$+2000$ (blue) kJ/mol.

In an EP, a constraint is applied, and this constraint is varied in regular small steps from the start to the final situation. All steps underwent full geometry optimization, applying the constraint. A plot of the (relative) energy versus the steps provides an impression of the feasibility of such a pathway. Figure 6 shows the case for the BF_3 catalyzed formation of iso THC, starting from Δ^9-CBD.
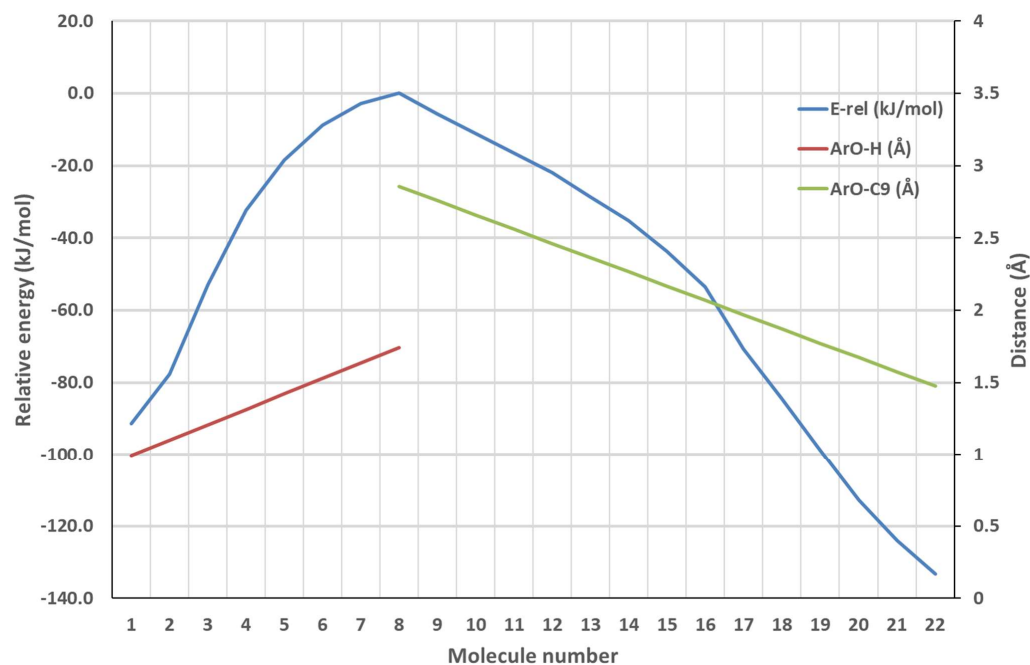

Figure 6. Combined energy profiles (B3LYP/6-31G*) for the BF_3 catalyzed formation of iso THC from Δ^9-CBD.

In Figure 6, two EPs are combined, both of which start from the geometry of the TS ring closure from Δ^9-CBD to iso Δ^8-THC, as shown in Figure 5. The first EP is the reverse of the proton transfer from $BF_3 \cdot \Delta^9$-CBD to the C10 of the cyclohexane ring. This EP ranges from molecule number 8 to 1, and the ArO–H distance changes in steps of ~0.1 Å from 1.743 Å

to 0.993 Å, the ArO–H equilibrium distance (red line). The second EP is the movement of the phenolic O to the C8 of the cyclohexane ring. This EP ranges from molecule number 8 to 22, and the ArO–C8 distance changes in steps of ~0.1 Å from 2.857 Å to 1.475 Å, the ArO–C8 equilibrium distance (green line). The energy curve (blue) does not show additional local maxima or minima. The Δ (E-total energy) from the TS ring closure iso THC to the product iso THC is −133.2 kJ/mol. A very similar EP was determined, showing the formation of Δ^8-CBD, the isomerized double bond product, from the TS ring closure iso THC. This energy curve does not show additional local maxima or minima. However, the Δ(E-total energy) from the TS ring closure iso THC to Δ^8-CBD is −92.0 kJ/mol. Therefore, in principle, fully reversible isomerization is very well possible but at sufficiently high reaction rates, the thermodynamic product, iso THC, will be formed exclusively.

3.2.4. Kinetic Models: Comparison of Computational and Experimental Results

Table 2 provides an overview of all activation barriers related to the conversion of Δ^9-CBD catalyzed by pTSA or $BF_3 \cdot Et_2O$. The table also contains pseudo-first-order rate constants based on the activation barriers only, and in the case of pTSA as catalyst, corrected pseudo-first-order rate constants. The derived rate constants were used in two simple kinetic models describing pTSA-catalyzed conversion of Δ^9-CBD to mainly Δ^8-THC and $BF_3 \cdot Et_2O$-catalyzed conversion of Δ^9-CBD to Δ^9-THC and iso THC.

Table 2. B3LYP/6-31G* activation barriers and pseudo-first-order reaction rate constants related to the conversion of Δ^9-CBD to Δ^8-THC, with pTSA and $BF_3 \cdot Et_2O$. In the pTSA case, T = 383.8 K (110.6 °C). In the $BF_3 \cdot Et_2O$ case T = 273.2 K (0.0 °C).

Molecular System	ν (1/cm)	ΔH_a (kJ/mol)	k (1/s)	k_c (1/s)
TS ring closure D^9 THC pTSA	i228	70.5	3.69×10^2	2.03×10^{-3}
TS ring closure D^8-THC pTSA	i99	57.5	2.19×10^{-4}	1.21×10^{-1}
TS concerted isomerization D^9->D^8-CBD pTSA	i100	75.3	8.21×10^{-1}	4.51×10^{-4}
TS concerted isomerization D^8->D^9-CBD pTSA	i100	86.8	2.23×10^0	1.23×10^{-5}
TS two-step isomerization D^9->D^8-CBD pTSA	i31	67.2	1.04×10^{-3}	5.71×10^{-3}
TS two-step isomerization D^8->D^9-CBD pTSA	i91	81.8	1.07×10^{-1}	5.88×10^{-5}
TS concerted isomerization D^9->D^8-THC pTSA	i152	95.7	1.37×10^{-1}	7.54×10^{-7}
TS concerted isomerization D^8->D^9-THC pTSA	i152	103.9	1.05×10^{-2}	5.77×10^{-8}
TS ring closure D^9-THC $BF_3 \cdot Et_2O$	i125	80.9	7.28×10^{-7}	
TS ring closure iso D^8-THC $BF_3 \cdot Et_2O$	i315	82.1	2.89×10^{-4}	

As discussed in the Materials and Methods section, reaction rates were calculated using:

$$k = k_0 \cdot [\text{catalyst}]/[\text{substrate}] \cdot e^{-Ha/RT} \ (1/s)$$

Thus, k represents a pseudo-first-order rate constant. As all transition state structures contain the catalyst, pTSA or BF_3, the pseudo-first-order rate constants were corrected for the [catalyst]/[substrate] ratio, which is the maximum amount of substrate that can react in time. The activation barriers for pTSA-catalyzed ring closure lead to rate constants that are orders of magnitude too high. It took some time before it was realized that pTSA in an apolar solvent under dry conditions is actually predominantly present as a dimer with a ΔH = −77.5 kJ/mol. The corresponding equilibrium constant K = 3.31×10^{10} and the fraction pTSA-monomer is 5.50×10^{-6} only. Correction for this small amount of monomeric pTSA led to the rate constants k_c, listed in the last column of Table 2.

For the case of catalysis with pTSA, a kinetic model was developed using the k_c values for ring closure Δ^9 THC pTSA, ring closure Δ^8-THC pTSA and two-step isomerization Δ^9->Δ^8-CBD pTSA only. These values are highlighted (green background) in Table 2. The concerted isomerization of Δ^9-CBD is not operative, as discussed above, and all other values for k_c are too low to play a role. Using the exact values shown in Table 2, a yield of 73.7% Δ^8-THC at a total conversion of Δ^9-CBD of 99.9% was predicted. It seems that overall selectivity to Δ^8-THC is slightly too low, while the overall conversion is slightly too high. Probably more important is the apparent absence of Δ^8-CBD in the reaction mixture after less than 15 min, which is in line with the experimental observation that Δ^8-CBD was not detected. Furthermore, the high selectivity to Δ^8-THC instead of Δ^9-THC is explained by the lower activation barriers for two-step isomerization from Δ^9-CBD to Δ^8-CBD and ring closure to Δ^8-THC. Adaptations of +2 kJ/mol in the activation barriers of ring closure of Δ^9 THC and ring closure of Δ^8-THC lead to an almost perfect fit, as can be seen in Figure 7. The fitted selectivity is 84% compared to 86% experimentally. Alternatively, the ΔH of dimerization of pTSA could be adapted, yielding a very similar result. It should be realized that such small adaptations are within the error limit of the calculations.
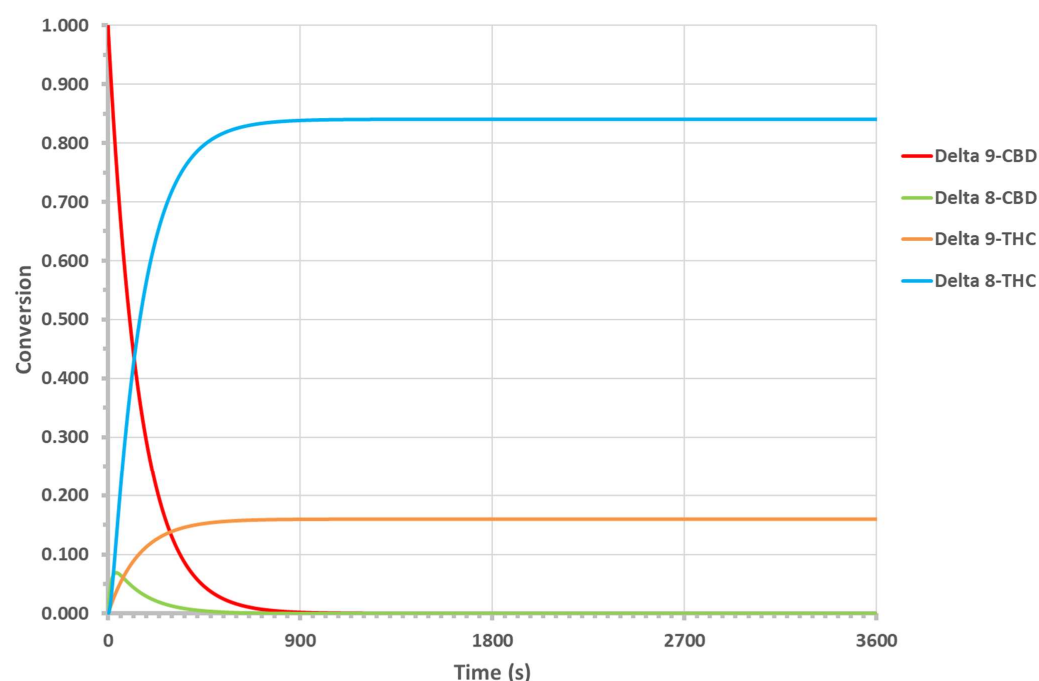

Figure 7. Fit kinetic model for formation of Δ^9 THC and Δ^8-THC, catalyzed by pTSA via two-step isomerization of Δ^9-CBD to Δ^8-CBD.

For the case of catalysis with $BF_3 \cdot Et_2O$, a kinetic model was developed using the k values for ring closure Δ^9 THC $BF_3 \cdot Et_2O$ and ring closure iso THC $BF_3 \cdot Et_2O$. These values are highlighted (green background) in Table 2. Using the exact values of Table 2, a yield of 61.9% Δ^9-THC and 36.5% iso THC was predicted at a total conversion of Δ^9-CBD of 98.5%. It seems that overall selectivity to Δ^9-THC is slightly too low, while the overall conversion is slightly too high. An adaptation from 80.9 to 81.5 kJ/mol of the activation barrier for ring closure to Δ^9 THC $BF_3 \cdot Et_2O$ and an adaptation from 82.1 to 83.5 kJ/mol of the activation barrier for ring closure to iso THC $BF_3 \cdot Et_2O$ leads to a perfect fit, with 66.6% Δ^9-THC and 27.6% iso THC and a total conversion of 94.2%.

4. Discussion and Conclusions

The basic research question of this study was the origin of the enormous difference in product selectivity between the catalysts pTSA and $BF_3 \cdot Et_2O$ in the conversion of

Δ^9-CBD. Molecular modeling was able to elucidate the mechanisms of pTSA- and $BF_3 \cdot Et_2O$-catalyzed ring closure and isomerization reactions of Δ^9-CBD.

In the pTSA case, the two mechanistic options for isomerization of an alkene with a sulfonic acid like pTSA are not new but go back to 1932. The two-step mechanism for isomerization is more favorable in this case because a tertiary carbenium ion is formed, and the pTSA-anion is stabilized by the phenolic OH-group. The activation barriers for ring closure of Δ^9-CBD and Δ^8-CBD to Δ^9-THC and Δ^8-THC are 70.5 and 57.5 kJ/mol, respectively, reflecting the relative stability of Δ^9-CBD over Δ^8-CBD, which is 11.8 kJ/mol. Using transition state theory and the earlier described expression for the reaction rate initially led to much too high reaction rates in the kinetic model. Later, it was realized that pTSA predominantly is present as a dimer in an apolar dry solvent. Correction for the correct amount of pTSA monomer led to reaction rates that predict amounts of Δ^9-THC and Δ^8-THC that a very close to the experimentally observed ones.

In the $BF_3 \cdot Et_2O$ case, it turned out that ring closure to Δ^9-THC and iso THC had to be taken into consideration only. Δ^9-THC and iso THC are formed exclusively because they are the thermodynamically favored products. Complexation with the Lewis acid BF_3 has turned the weakly acidic phenol into a powerful Brønsted acid, capable of completely protonating the alkene groups. The use of computational activation barriers to calculate pseudo-first-order reaction rates led to an almost perfect fit of the kinetic model with the experimental data.

In summary, the application of molecular modeling using standard DFT quantum chemical calculations and transition state theory to estimate reaction rates led to a qualitative and quantitative understanding of the underlying reaction mechanisms and various experimentally formed reaction products.

With respect to the larger field of cannabinoid research, or even more generally, the field of natural product research, it can be concluded that presently, a molecular modeling approach is capable of qualitatively directing research to selective chemical transformations of substrates with multiple substituents with a similar reactivity. Still a limited amount of experimental work is needed to calibrate the computational results. After such calibration, even meaningful quantitative predictions can be made. The molecular modeling approach consists of the step-by-step application of relatively well-validated methods, ranging from molecular mechanics to quantum mechanics, such as density functional theory.

References

1. Google Trends. Available online: https://trends.google.de/trends/explore?q=CBD&geo=DE&date=2013-01-01%202020-03-11#TIMESERIES (accessed on 27 December 2023).
2. Golombek, P.; Müller, M.; Bartholt, I.; Sproll, C.; Lachenmeier, D.W. Conversion of cannabidiol (CBD) into psychotropic cannabinoids including tetrahydrocannabinol (THC): A controversy in the scientific literature. *Toxics* **2020**, *8*, 41. [CrossRef] [PubMed]
3. PubChem, National Library of Medicine, Cannabidiol, PubChem CID 644019. Available online: https://pubchem.ncbi.nlm.nih.gov/compound/644019 (accessed on 27 December 2023).
4. Healthline. Available online: https://www.healthline.com/health/cbd-vs-thc#_noHeaderPrefixedContent (accessed on 1 March 2024).

5. Nelson, K.M.; Bisson, J.; Singh, G.; Graham, J.G.; Chen, S.-N.; Friesen, J.B.; Dahlin, J.J.; Niemitz, M.; Walters, M.A.; Pauli, G.F. The essential medicinal chemistry of cannabidiol (CBD). *J. Med. Chem.* **2020**, *63*, 12137–12155. [CrossRef] [PubMed]

6. Buijs, W. The scientific controversy on the conversion of CBD into THC in the human stomach: Molecular modelling and experimental results compared. *Forensic Chem.* **2023**, *32*, 100467. [CrossRef]

7. UN Commission on Narcotic Drugs Reclassifies Cannabis to Recognize Its Therapeutic Uses. Available online: https://www.who.int/news/item/04-12-2020-un-commission-on-narcotic-drugs-reclassifies-cannabis-to-recognize-its-therapeutic-uses (accessed on 17 January 2024).

8. Webster, G.B.; Sarna, L.P.; Mechoulam, R. Conversion of CBD to Delta8-THC and Delta9-THC. US 2004/0143126A1, 22 July 2004.

9. Webster, G.B.; Sarna, L.P.; Mechoulam, R. Conversion of CBD to Δ8-THC and Δ9-THC. US 7,399,872 B2, 15 July 2008.

10. PubChem, National Library of Medicine, DELTA8-Tetrahydrocannabinol PubChem CID 2977. Available online: https://pubchem.ncbi.nlm.nih.gov/compound/2977 (accessed on 15 February 2024).

11. Wavefunction, Inc. Available online: www.wavefun.com (accessed on 27 December 2023).

12. Halgren, T.A. Merck molecular force field. I. Basis, form, scope, parameterization, and performance of MMFF94. *J. Comput. Chem.* **1996**, *17*, 490–519.

13. Halgren, T.A. Merck molecular force field. II. MMFF94 van der Waals and electrostatic parameters for intermolecular interactions. *J. Comput. Chem.* **1996**, *17*, 520–552.

14. Halgren, T.A. Merck molecular force field. III. Molecular geometries and vibrational frequencies for MMFF94. *J. Comput. Chem.* **1996**, *17*, 553–586. [CrossRef]

15. Halgren, T.A.; Nachbar, R.B. Merck molecular force field. IV. conformational energies and geometries for MMFF94. *J. Comput. Chem.* **1996**, *17*, 587–615. [CrossRef]

16. Halgren, T.A. Merck molecular force field. V. Extension of MMFF94 using experimental data, additional computational data, and empirical rules. *J. Comput. Chem.* **1996**, *17*, 616–641. [CrossRef]

17. Hehre, W.J.; Ditchfield, R.; Radom, L.; Pople, J.A. Molecular orbital theory of the electronic structure of organic compounds. V. Molecular theory of bond separation. *J. Am. Chem. Soc.* **1970**, *92*, 4796.

18. Ptáček, P.; Šoukal, F.; Opravil, T. *Introduction to the Transition State Theory*; Open Research; IntechOpen: London, UK, 2018; Chapter 2. [CrossRef]

19. Virant, M.; Drvaric Talian, S.; Podlipnik, C.; Hribar-Lee, B. Modelling the correlation between molecular electrostatic potential and pK_a on sets of carboxylic acids, phenols and anilines. *Acta Chim. Slov.* **2017**, *64*, 560–563. [CrossRef]

20. Goddard, A.R.; Apebende, E.A.; Lentz, J.C.; Carmichael, K.; Taresco, V.; Irvine, D.J.; Howdle, S.M. Synthesis of water-soluble surfactants using catalysed condensation polymerisation in green reaction media. *Polym. Chem.* **2021**, *20*, 2992–3003. [CrossRef] [PubMed]

21. Whitmore, F.C. The common basis of intramolecular rearrangements. *J. Am. Chem. Soc.* **1932**, *54*, 3274. [CrossRef]

22. Ipatieff, V.N.; Corson, B.B. Catalytic polymerization of gaseous olefins by liquid phosphoric acid. Butylene. *Ind. Eng. Chem.* **1935**, *27*, 1069. [CrossRef]

23. Cabré, A.; Rafael, S.; Sciortino, G.; Ujaque, G.; Verdaguer, X.; Lledós, A.; Rier, A. Catalytic Regioselective Isomerization of 2,2-Disubstituted Oxetanes to Homoallylic Alcohols. *Angew. Chem. Int. Ed.* **2020**, *59*, 7521. [CrossRef] [PubMed]

24. Posner, G.H.; Shulman-Roskes, E.M.; Oh, C.H.; Carry, J.-C.; Green, J.V.; Brian-Clark, A.; Dai, H.; Anjeh, T.E.N. BF_3-OEt_2 promotes fast, mild, clean and regioselective dehydration of tertiary alcohols. *Tetrahedron Lett.* **1991**, *32*, 6489–6492. [CrossRef]

25. Kustiana, B.A.; Elsherbeni, S.A.; Linford-Wood, T.G.; Melen, R.L.; Grayson, M.N.; Morrill, L.C. $B(C_6F_5)_3$-Catalyzed E-Selective Isomerization of Alkenes. *Chem. Eur. J.* **2022**, *28*, e202202454. [CrossRef] [PubMed]

26. Buijs, W. Role of Fe Complexes as Initiators in the Oxidative Degradation of Amine Resins for CO_2 Capture: Molecular Modeling and Experimental Results Compared. *ACS Eng. Au* **2023**, *4*, 112–124. [CrossRef]